Energy & Environmental Science

"Water-in-salt" Polymer Electrolyte for Li-ion Batteries

Journal:	*Energy & Environmental Science*
Manuscript ID	EE-COM-05-2020-001510.R1
Article Type:	Communication
Date Submitted by the Author:	14-Jul-2020
Complete List of Authors:	Wang, Chunsheng; University of Maryland at College Park Zhang, Jiaxun; University of Maryland at College Park Cui, Chunyu; University of Maryland at College Park Wang, Peng-Fei ; University of Maryland at College Park, Li, Qin; University of Maryland at College Park Chen, Long; University of Maryland at College Park Han, Fudong; University of Maryland at College Park Jin, Ting; University of Maryland at College Park Liu, Sufu; University of Maryland at College Park Choudhary, Hema; University of Maryland at College Park Raghavan, Srinivasa; University of Maryland, Chemical and Biomolecular Engineering Eidson, Nico; University of Maryland, Department of Chemical & Biomolecular Engineering Cresce, Arthur; U. S. Army Research Laboratory, Electrochemistry Ma, Lin; U. S. Army Research Laboratory, Electrochemistry Uddin, Jasim; LIOX power.Inc Addison, Dan; LIOX power.Inc Yang, Chongyin; University of Maryland at College Park,

Broader context

Safety is the most important factor for rechargeable batteries especially in terms of wearable devices and electrical transportations. Aqueous electrolytes possess the merit of intrinsic safety, while the narrow (< 2 V) long-duration operation voltage of traditional aqueous electrolyte is a critical bottleneck for high energy density safety Li-ion batteries. The revolutionary "water-in-salt" electrolyte (WiSE) further broadened the long-duration operation voltage, still, most of high capacity anodes are not workable in WiSE owing to hydrogen evolution reaction of water on anodes. Herein, we reported a polymer stabilized WiSE structure, which cooperated solid-state aqueous polymer electrolyte (SAPE) with a localized strongly basic solid polymer electrolyte (SPE) on anode. The solid-state electrolyte demonstrate the concept of solid state battery is achievable by fabricating high-voltage stacking cell and fabricating ultra-thick electrode. A Li-ion battery based on capacity matched $LiMn_2O_4/Li_4Ti_5O_{12}$ was demonstrated to deliver an unprecedented high reversibility of charge/discharge capacities at a low current density in battery. This newly developed reduced salt concentration WiSE not only reduces the cost of aqueous electrolyte, but also opens up another perspective on future directions and guidance for the design of aqueous electrolyte for high-energy-density Li-ion batteries in practical applications.

Highlights

An extended ESW of 3.86 V is achieved at 12 mol kg^{-1} SAPE

The LMO/LTO full cell exhibit an unprecedented high initial CE of 90.50%

A dense $LiF\text{-}Li_2CO_3$ SEI was detected on anode surface

High-voltage bipolar cell is fabricated to demonstrate aqueous solid state battery

TOC

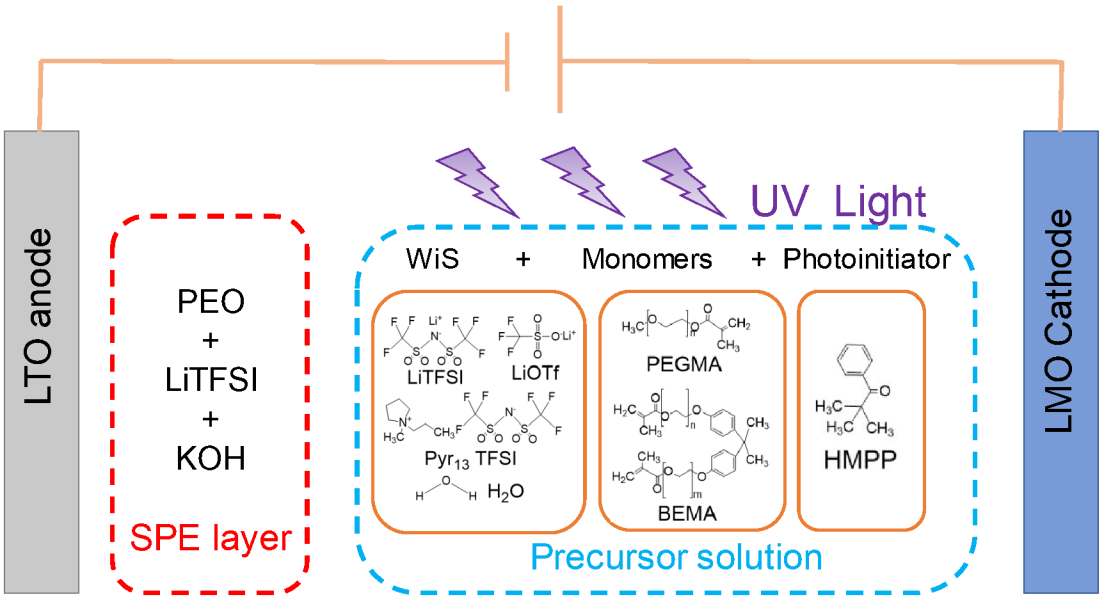
LTO anode
PEO
+
LiTFSI
+
KOH
SPE layer
UV Light
WiS + Monomers + Photoinitiator
LiTFSI
LiOTf
Pyr13 TFSI
H2O
PEGMA
BEMA
HMPP
Precursor solution
LMO Cathode

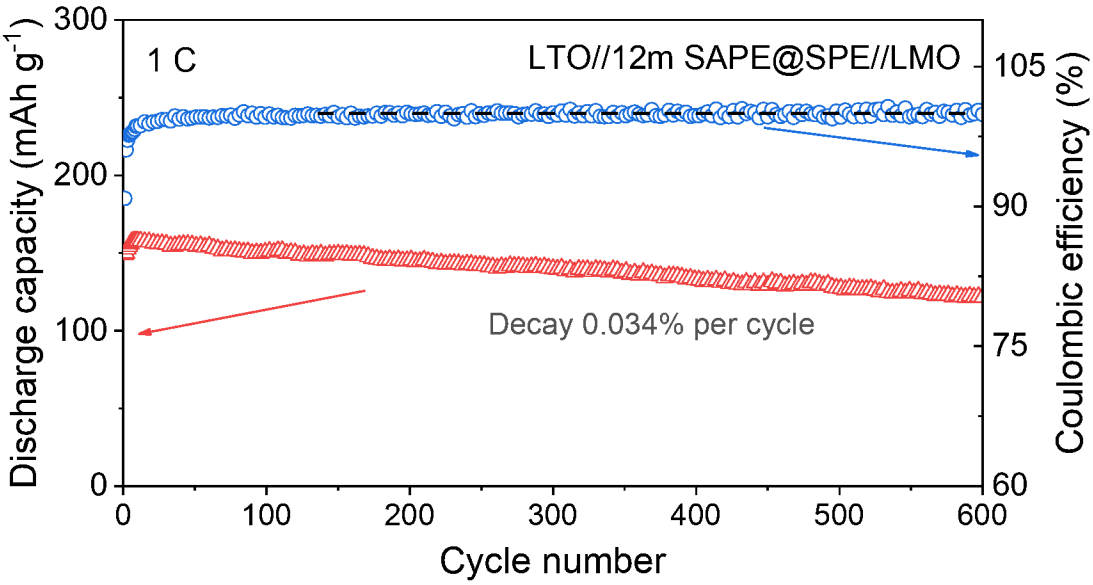
1 C
LTO//12m SAPE@SPE//LMO
Decay 0.034% per cycle
Discharge capacity (mAh g-1)
Coulombic efficiency (%)
Cycle number
0
100
200
300
400
500
600
60
75
90
105

"Water-in-salt" Polymer Electrolyte for Li-ion Batteries

Jiaxun Zhang[a‡], Chunyu Cui[a‡], Peng-Fei Wang[a‡], Qin Li[a], Long Chen[a], Fudong Han[a], Ting Jin[a], Sufu Liu[a], Hema Choudhary[a], Srinivasa R. Raghavan[a], Nico Eidson[ab], Arthur von Cresce[b], Lin Ma[b], Jasim Uddin[c], Dan Addison[c], Chongyin Yang[a*], Chunsheng Wang[ad*]

[a]. *Department of Chemical and Biomolecular Engineering, University of Maryland, College Park, MD 20742, USA*

[b]. *Department Electrochemistry Branch, Sensor and Electron Devices Directorate, Power and Energy Division, US Army Research Laboratory, Adelphi, MD 20783, USA*

[c]. *Liox Power, Inc., Pasadena, CA, 90065, USA*

[d]. *Department of Chemistry and Biochemistry, University of Maryland, College Park, MD 20742, USA*

† Electronic Supplementary Information (ESI) available: See DOI: 10.1039/x0xx00000x

‡ These authors contributed equally.

* *Corresponding author.*

Email: cswang@umd.edu, cyyang@umd.edu

Abstract

Recent success in extending the electrochemical stability window of aqueous electrolytes to 3.0 V by using 21m "water-in-salt" (WiS) has raised a high expectation for developing safe aqueous Li-ion batteries. However, the most compatible $Li_4Ti_5O_{12}$ anodes still cannot use in WiS electrolyte due to the cathodic limit (1.9 V vs. Li/Li^+). Herein, a UV-curable hydrophilic polymer is introduced to further extend the cathodic limit of WiS electrolytes and replace separator. In addition, a localized strongly basic solid polymer electrolyte (SPE) layer is coated on anode to promote the formation of LiF-rich SEI. The synthetic impacts of UV-crosslink and local alkaline SPE on anodes extend the electrochemical stability window of the solid-state aqueous polymer electrolyte to ~ 3.86 V even at a reduced salt concentration of 12 mol kg^{-1}. It enables a separator-free $LiMn_2O_4//Li_4Ti_5O_{12}$ aqueous full cell with a practical capacity ratio (1.14) of cathode and anode to deliver a steady energy density of 151 Wh kg^{-1} at 0.5 C with initial Coulombic efficiency of 90.50% and cycle for over 600 cycles with average Coulombic efficiency of 99.97%, which was never reported before for aqueous $LiMn_2O_4//Li_4Ti_5O_{12}$ full cell. This flexible and long-duration aqueous Li-ion battery with hydrogel WiSE can be widely used as the power sources in wearable devices and electrical transportations where both energy

density and battery safety are of high priority. An ultra-thick LTO electrode with UV-curable polymer electrolyte as binder is demonstrated as solid state battery electrode. And a high-voltage (7.4 V) solid-state bipolar cell is assembled with solid-state UV-curable polymer as electrolyte.

Keywords

Aqueous Li-ion battery, Water-in-salt, Solid-state aqueous polymer electrolyte, Solid polymer electrolyte, Nonflammable, Bipolar battery

Introduction

The state-of-the-art Li-ion batteries have been dominated storage market for electronic devices and electrical vehicles owing to their high energy density of 250 Wh kg^{-1} and long cycle life. However, the use of flammable non-aqueous electrolyte Li-ion batteries has raised serious safety concerns. Replacing flammable electrolytes with aqueous electrolytes will bring intrinsic safety and reduce materials and manufacturing costs. Unfortunately, aqueous Li-ion batteries suffer from low energy density due to the narrow (< 2 V) electrochemical stability window (ESW) of the electrolyte. Recently, the ground-breaking of "water-in-salt" electrolyte (WiSE) successfully expanded the ESW of water to 3.0 V.[1-4] To enhance energy density of WiSE batteries, the catholic limitation of 1.9 V needs to be further reduced, and a high Coulombic efficiency (CE) of > 99.9% at a matched areal capacities of cathode/anode at a low charge/discharge rates is required for a long-term cycling. Up till now, such a high CE has not been achieved in 3V-class full cells, e.g. $LiMn_2O_4//Li_4Ti_5O_{12}$.

The effective strategies for suppressing parasitic reaction on electrodes in WiSE are (1) reducing water activity by minimizing the water molecules in Li^+ ion solvation shell in the bulk electrolytes and (2) passivating the anode by forming LiF-rich solid electrolyte interphase (SEI) from reduction of LiTFSI salt.[1, 5] However, due to the solubility limitation,[6] further reducing the water molecule in Li^+ ion solvation shell is quite a challenge. For this aspect, adding highly hydrophilic polymer network as water stabilizer can further extend the thermodynamic stability window of WiSE and reduce the decomposition kinetics of water.[7] The molecular dynamics study of polymer-water interaction in hydrogels demonstrated that the mobility of water molecules is significantly lowered around polymer chains.[8] The NMR characterization also

confirmed that the water component appears to be tightly bound to the cross-linked polymer networks.[9] The suppressing of water molecule mobility in the cross-linked polymer network will reduce the water activity, thus extending the stability window.

UV-curing is a mature polymerization technique and has been widely utilized in the domain of photolithography for the production of optical and electronic devices, biomedical applications and energy storage systems[10-12] owing to the feature of easy, low cost, fast and reliable.[13] Under UV irradiation, a liquid poly-functional monomer reacts with a proper photo-initiator forming a solid cross-linked film. UV-cured methacrylic membranes have been used as GPE for lithium ion batteries several years ago.[14, 15] Flexible 3D networks have been fabricated by the UV-curing technology, which shown great potential for large scale application.

In this work, by incorporating WiSE with UV-curable methacrylic polymer, we designed a solid-state aqueous polymer electrolyte (SAPE), in which the abundant hydrophilic groups stabilized water molecules due to the sluggish water mobility in SAPE and formed a water-less thin passivation interphase between anode and electrolyte. Moreover, the anode was pre-coated with a strongly basic water-free solid polymer electrolyte to further promote the formation of passivation interphase.[16] All of these promoted formation of a more robust SEI to reduce the water reduction reactions on anode surface. The electrochemical stability window of aqueous electrolytes was extended from 3.0 V of 21m WiSE to ~ 3.86 V of 12m UV-cured SAPE. Using a 3 V class $LiMn_2O_4$//$Li_4Ti_5O_{12}$ (LMO//LTO) full cell with capacity ratio Q_c/Q_a of 1.14 and areal capacity of 0.5 mAh cm^{-2} as a demo cell, the UV-cured SAPE enables LMO//LTO full cell to achieve an energy density of 151 Wh kg^{-1} at 0.5 C with initial Coulombic efficiency of 90.50% and cycled for over 600 cycles with average Coulombic efficiency of 99.97%.

Results and discussions

Synthesis and property of SAPEs

The synthesis procedure of the solid-state aqueous polymer electrolytes is demonstrated in Fig. 1a. A methacrylic based di-functional oligomer, Bisphenol A ethoxylate dimethacrylate (BEMA, M_w = 1700) was used as a cross-linker.[15] Poly(ethylene glycol) methyl ether

methacrylate (PEGMA, M_w = 500) was used as a reactive diluent to enhance the mobility of lithium ions in the polymer matrix.[15] 2-hydroxy-2-methylpropiophenone (HMPP) functioned as a photo-initiator. Firstly, the precursor solution was prepared by dissolving different salt (LiTFSI, LiOTf, Pyr_{13}TFSI) into water and monomers (Fig. 1a). The precursor solution is transparent due to the miscibility between water, monomers and salts. Then, the precursor solution was cross-linked by exposing it to UV light (wavelength ~ 400 nm) for 90 secs to induce photopolymerization of the methacrylic groups and form solid-state aqueous polymer electrolyte (SAPE) (Fig. S1, ESI†). The crosslinking process is realized by the conversion of double bond (>C=C<) during exposure of UV light (Fig. 1a). As a one-pot synthesis method, the UV-cured polymerization process possesses the merit of facile and high efficiency. Two type SAPEs were fabricated. One is 11m LiTFSI-LiOTf-H_2O-polymer SAPE (11m SAPE) that is obtained by dissolving 8.5m LiTFSI and 2.5m LiOTf into monomers and water (m is mol kg^{-1}). The second type SAPE is 12m LiTFSI-LiOTf-Pyr_{13} TFSI-H_2O-polymer SAPE (12m SAPE) that is achieved by dissolving 5.2m LiTFSI, 5m Pyr_{13} TFSI and 1.8m LiOTf into monomers and water. LiTFSI and LiOTf facilitate the formation of hydrophobic LiF SEI.[17] Since Pyr_{13} TFSI is non-volatility and non-flammable,[18] it was introduced into 12m SAPE to further lower the water activity and change the solvation structure around Li^+.[19] The detailed weight ratio of each component in the system is presented in Table S1 (ESI†).

The thermal stability of 11m SAPE and 12m SAPE is evaluated with differential scanning calorimetry (DSC), and compared to 28 m (21m-LiTFSI-7m LiTOf) liquid WiSE. Both SAPEs show high thermos-stability with no significant exothermic peak observed before 350 °C, which is essentially identical to that of 28m WiSE (Fig. S2, ESI†). Moreover, water-retention in 12m SAPE is evaluated at real ambient condition (room temperature). As shown in Fig. S3 (ESI†), the mass of 12m SAPE gradually increases during the first few hours, owing to the moisture abstraction from the ambient (the air humidity around 60%). After that the weight remains a constant. Thus, the 12m SAPE performs superior ability to maintain water inside of the polymer framework even under the ambient environment.

The ionic conductivities of 28m WiSE, 11m SAPE and 12m SAPE at various temperatures are presented in Fig. 1c. At room temperature (25 °C), the ionic conductivities of 28m WiSE, 11m SAPE and 12m SAPE are 7.5 mS cm^{-1}, 3.0 mS cm^{-1} and 1.7 mS cm^{-1}, respectively.

Although the ionic conductivities of 11m SAPE and 12m SAPE at room temperature are slightly lower than the non-aqueous electrolyte (10.7 mS cm^{-1} for 1.0 M $LiPF_6$ in EC/DMC at 25 °C[20]) and the liquid WiSE electrolyte (10.0 mS cm^{-1} for 21m LiTFSI in water at 25 °C[1]), they are still 2 orders of magnitude larger than those best solid polymer electrolytes (4.4 × 10^{-5} S cm^{-1} for SiO_2 modified PEO-$LiClO_4$ SPE at 30 °C).[21, 22]

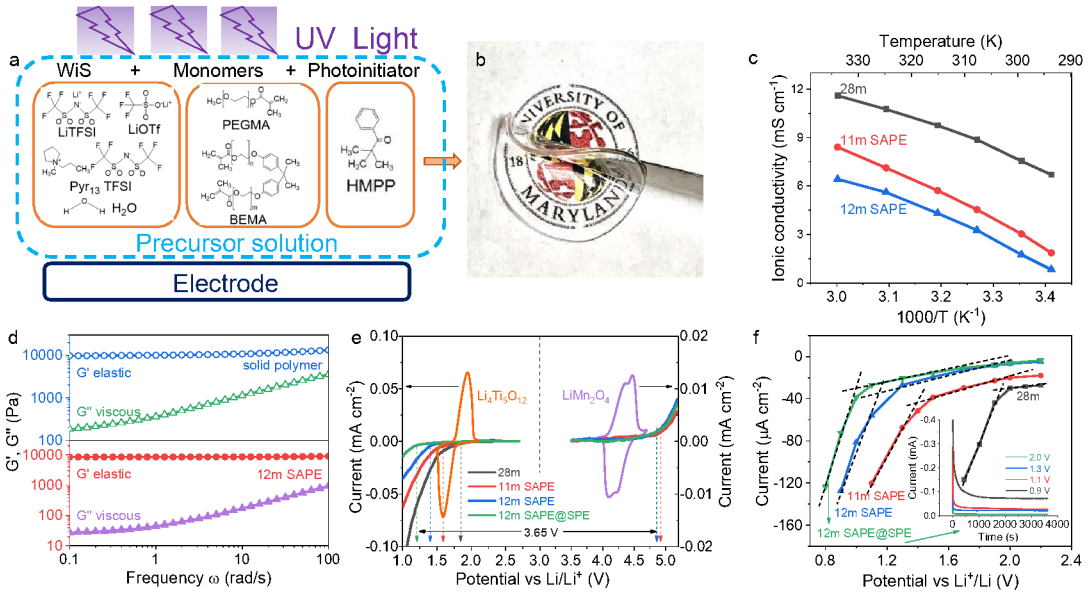

Figure 1 Schematic of SAPE synthesis procedure and properties of the synthesized SAPEs. (a) Chemical structure of the compositions used to synthesize solid-state aqueous polymer electrolyte networks. And schematic exemplifying the concept of *in situ* crosslinking on an electrode. (b) Prototype of a typical SAPE network. (c) The temperature dependence of ionic conductivities in the range of 20 to 60 °C for 28m WiSE, 11m SAPE and 12m SAPE. (d) Oscillatory shear rheology of solid polymer and 12m SAPE, the elastic modulus G' and the viscous modulus G'' are plotted as functions of the frequency ω. (e) The linear sweep voltammetry of different electrolytes (28m WiSE, 11m SAPE, 12m SAPE) at scanning rate of 0.1 mV s^{-1}. (Electrode area: 0.5 cm^2) PEO-LiTFSI-KOH SPE is coated on Al foil electrode to measure the cathodic limit for 12m SAPE@SPE electrolyte. The working electrodes were Al for the cathodic limit, the working electrodes were Ti for the anodic limit. Cyclic voltammetry (CV) of $Li_4Ti_5O_{12}$ (LTO) and Li_2MnO_4 (LMO) scanned at 0.1 mV s^{-1} in 12m SAPE are also presented. (f) Chronoamperometry of different electrolytes (28m WiSE, 11m SAPE, 12m SAPE and 12m SAPE@SPE electrolyte) on Al foil electrode. Different potentials are applied on Al working electrode, the steady state current lined in one curve. The current-time curve of the 12m SAPE@SPE electrolyte is presented in the inset.

The mechanical property of solid-state aqueous polymer electrolyte (12m SAPE) is studied by oscillatory shear (detailed in the Supporting Information),[23] and compared it with the solid polymer (10 wt% BEMA and 90 wt% PEGMA). Fig. 1d presents the frequency (ω) response of the elastic modulus G' and viscous modulus G''. The elastic modulus G' of both SAPE and solid polymer are much larger than their viscous modulus G''. In addition, the

modulus G' is independent of frequency and G'' is gradually increase with frequency (ω), suggesting that the SAPE is more like solid electrolytes rather than the liquid electrolytes. The value of elastic modulus G' is the crucial parameter as it is the modulus of the polymer under shear (in the linear viscoelastic region). G' of solid polymer is 10 kPa, and G' of 12m SAPE is 8.5 kPa (both values applies to a frequency of 1 rad s^{-1}). The elastic modulus of 12m SAPE is very close to the solid polymer, and is high enough to use as a separator to prevent the contact of anode and cathode electrode. As depicted in Fig. S4 and video S1 (ESI†), SAPE exhibits good stretchability even after the length of SAPE is extended to nearly 200%, demonstrating excellent flexibility of the SAPE.

The electrochemical stability windows of 28m WiSE, 11m SAPE, 12m SAPE are compared by linear sweep voltammetry (LSV) at a scanning rate of 0.1 mV s^{-1} using non-active Titanium (Ti) foil or Al foil as current collectors. As shown in Fig. 1e and Fig. S5a, the hydrogen evolution potential of 28m WiSE, 11m SAPE and 12m SAPE is 1.83 V, 1.59 V and 1.41 V, respectively. Therefore, the cathodic limit of 11m SAPE electrolyte negatively extends by 0.24 V is due to the high salt concentration and polymer framework as water stabilizer. The further extension of ESW for 12m SAPE is due to the cooperation of high lithium salt concentration, polymer framework and ionic liquid. Besides, a strongly basic water-free polymer electrolyte was pre-coated on Al foil to further expand the electrochemical stability window (ESW) of 12m SAPE. The pre-coated solid polymer electrolyte (SPE) composed of PEO, LiTFSI and KOH with the weight ratio of 0.55:0.25:0.2, denoted as SPE. The hydrogen evolution potential on Al after SPE coating is further negatively shifted to 1.21 V. To eliminate kinetics effect, the stricter ESW measurements using the chronoamperometry is conducted. Specifically, a constant potential is imposed on the working electrode and the current is recorded with time until the current reaches a steady state. The current-time curves of Al electrodes at different potential in 28m WiSE, 11m SAPE and 12m SAPE are presented in Fig. S5 (ESI†). At the steady state, the onset of rapidly raising current is only attributed to the side reaction of hydrogen evolution reaction (HER). The cathodic limit of 12m SAPE@SPE can be negatively extended to 1.0 V from the chronoamperometry analysis (Fig. 1f). The extension of cathodic limit is due to the suppression of water molecules activities within the cross-linked solid-state polymer network and highly-concentrated salt as discussed in the late section. The

anodic limit of 11m SAPE and 12m SAPE are 4.87 V and 4.86 V, respectively, which is 4 mV less than 28m WiSE due to the oxidation of solid polymer electrolyte at high voltage (Fig. 1e).[15] Overall, an electrochemical stability window of 3.86 V was achieved for the 12m SAPE@SPE electrolyte. Since the redox reaction potentials of LMO cathode and LTO anode shifted ~200 mV positively in the high concentration electrolyte, the redox reaction potentials of LMO and LTO are completely inside of the ESW of 11m SAPE, 12m SAPE, and 12m SAPE@SPE electrolytes, which will potentially achieve high CEs.

High reversibility of LTO in solid-state aqueous polymer electrolytes

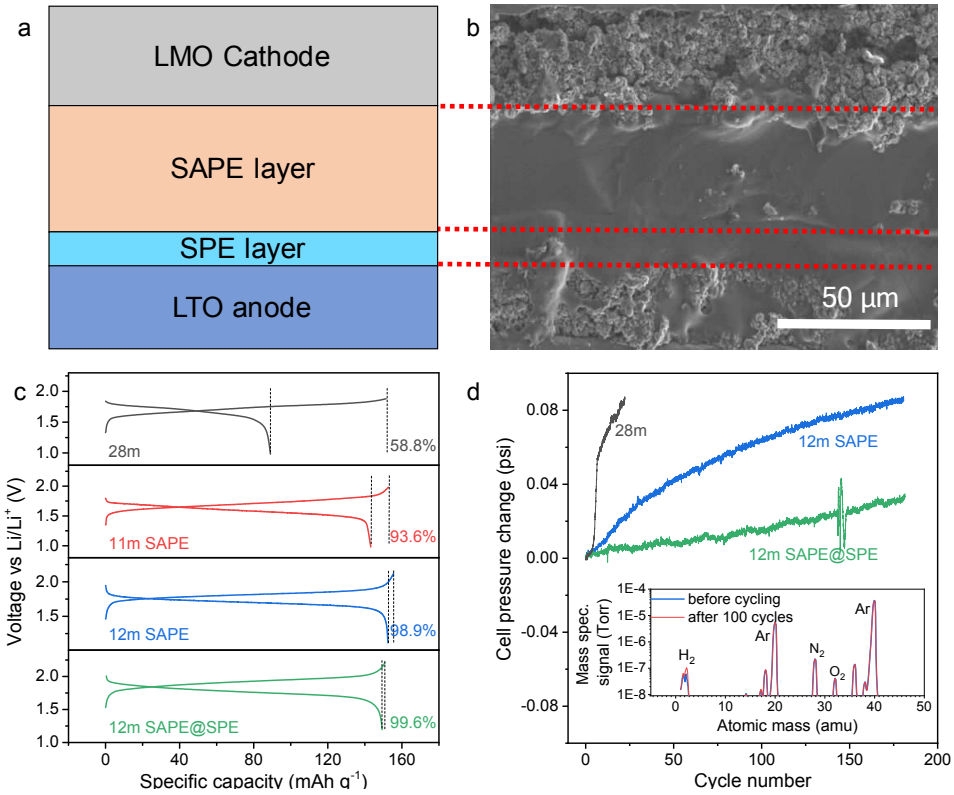

Figure 2 Schematic and reality of LMO//LTO full cell structure, Coulombic efficiency of LTO anode and *in-situ* monitoring of internal gas pressure change for the full cell. (a) Schematic structure of LMO/SAPE layer/SPE layer/LTO cell. (b) Cross-section SEM image of LMO//LTO full cell with 12m SAPE and PEO-LiTFSI-KOH SPE layer (LMO anode (~35 μm); SAPE layer (~42 μm); SPE layer (~8 μm); LTO anode (~28 μm)). (c) Voltage profiles for the 10th cycle charge-discharge profiles (0.5 C) of full cells constructed with Li_2MnO_4 cathode and $Li_4Ti_5O_{12}$ anode in 28m WiSE (2nd cycle), 11m SAPE, 12m SAPE and 12m SAPE@SPE electrolyte. The capacity ratio of LMO//LTO is set as 3:1, the Coulombic efficiency of the full cell is presented as the efficiency of LTO anode. (d) *In-situ* monitoring of internal gas pressure change for LMO//LTO full cell with various electrolytes during long cycling, revealing the amount of H_2 gas evolution. Inset: The gas compositions examined by mass spectra before and after cycling for LMO//LTO full cell with 12m SAPE@SPE electrolytes.

Fig. 2a shows the schematic diagram of LMO/SAPE@SPE/LTO cell, and Fig. 2b shows the cross-section SEM image of LMO/12m SAPE@SPE/LTO cell. The CE of LTO in different electrolytes is evaluated using excess LMO as counter electrode (LMO//LTO capacity ratio of 3:1) in coin cells. As presented in Fig. 2c, the CE of LTO at the second cycle in 28m WiSE is only 59% owing to the rapid side reaction of hydrogen evolution reaction (HER). After introduction of polymer into water-in-salt electrolyte to form the solid-state aqueous polymer electrolyte, the CE of LTO in 11m SAPE and 12m SAPE increase to 93.6% and 98.9 % after 10 cycles, respectively. The introduction of PEO-LiTFSI-KOH SPE layer between LTO and 12m SAPE electrolyte further enhance the CE of LTO to 99.6 % after 10 cycles, indicating the side reaction of HER on LTO is effectively suppressed by PEO-LiTFSI-KOH SPE layer. In order to quantitatively study the HER during the cycling of LMO//LTO full cell, an in-situ cell pressure analysis is monitored (Fig. 2d). The increase in cell pressure during charge/discharge cycles demonstrates the production of hydrogen gas inside of the cell, which is confirmed by mass spectra analysis. The cell pressure increased rapidly in 28m WiSE, while the increase of the cell pressure in 12m SAPE and 12m SAPE@SPE electrolytes are very slow, especially in 12m SAPE@SPE electrolytes. The gas composition of 12m SAPE@SPE electrolytes is analyzed with mass spectrometry. Comparing the gas composition in the fresh cell and in the cell after 100 cycles in 12m SAPE@SPE electrolytes, only hydrogen gas increased, indicating the increase of cell pressure during cycling is contributed by HER. The increase of pressure in SAPE@SPE electrolyte is mainly attributed to hydrogen evolution during SEI formation process in the initial 10 cycles. It should be noted that very small amount of H_2 generated in 100 cycles (7.6×10^{-8} mol mAh^{-1}), which is comparable with the gas amount generated in state-of-the-art non-aqueous LMO//LTO full cell during cycling.[24]

The mechanism for the suppression of hydrogen evolution reaction is investigated using Fourier transformed infrared (FTIR) spectra, Raman and X-ray photoelectron spectroscopic (XPS). The water activities in 11m and 12m SAPE and methacrylic based solid polymer are characterized using FTIR. Fig. 3a presents FTIR spectra of water in solid polymer (10 wt% BEMA and 90 wt% PEGMA) to demonstrate the O-H stretching vibration modes of water molecules, which will reveal their hydrogen bond association.[2, 25] As a reference, the FTIR of pure water presents fine structures of the featured broad band, consisting of several components

attributed to various water molecules with different hydrogen-bonding environments in water clusters.[2, 6, 25] Specifically, the O-H stretching band can be deconvoluted into several Gaussian peaks corresponding to hydrogen-bonded water molecules with different donor (D) and acceptor (A) hydrogen bonds. The FTIR spectra of H_2O can be deconvoluted into five sub-bands, located at 3028, 3225, 3405, 3551 and 3637 cm^{-1}, which are assigned to O-H vibrations engaged in DAA, DDAA, DA, DDA hydrogen-bonding and free O-H vibrations. The FTIR of solid polymer with 6% and 10% of water was first analyzed as a control electrolyte to compare with the SAPE. For the solid polymer with 10% of water, three Gaussian peaks centered at 3278, 3458 and 3561 cm^{-1} are assigned for deconvolution of this area. The position of bands at 3278 cm^{-1} and 3458 cm^{-1}, corresponding to DDAA and DA stretching vibrations are slightly shifted in respect to the peaks of water. The peak centered at around 3561 cm^{-1} represents the superposition of DDA and free O-H stretching vibration. The disappearance of DAA and weaken of free O-H stretching vibration demonstrates that polymer matrix successfully stables the water molecules, dramatically depressing the activity and mobility of water molecules. The stretching vibrations of solid polymer with 6% water is similar to that of solid polymer with 10% of water, but the peak position moved more close to the stretching vibration of DA, which indicates that large water clusters is reduced.[26]

The FTIR of different aqueous electrolytes in Fig. 3b shows typical stretching mode of the O-H vibration peak (3,000-3,800 cm^{-1}). The 1m LiTFSI in H_2O shows an similar spectrum as pure water, which can be deconvoluted into five sub-bands,[27] located at 3156, 3251, 3397, 3512, 3612 cm^{-1} (H_2O), which are assigned to O-H vibrations engaged in DAA, DDAA, DA, and DDA hydrogen-bonding, and free O-H vibrations. The blue shift of the O-H covalent bond oscillation is attributed to the perturbation of water hydrogen bond network with lithium salt around it. For the 28m WiSE, four Gaussian peaks can be deconvoluted in this area. The disappear of DAA stretching vibrations at 3028 cm^{-1} verified that mobility of water molecular is constrained within 28m highly-concentrated salt aqueous electrolyte. Three Gaussian peaks can be deconvoluted for the 11m SAPE and 12m SAPE, comparing with 28m WiSE, low-frequency portions demise to high-frequency ones in 12m SAPE, indicating oxygen groups on polymers further break down the water-rich cluster size[28] and reduce the activity of water molecules. Furthermore, Raman spectra is adopted to characterize the structure of aqueous

electrolytes. As summarized in Fig. S6a (ESI†), the O-H vibration peak at 3560 cm^{-1} gradually disappears from 28m WiSE to 12m SAPE, which is in accordance with the FTIR results. Consequently, the water activity is severely reduced in 12m SAPE under the cooperation of cross-linked solid-state polymer network and highly-concentrated salt, and then the CE will be greatly improved.

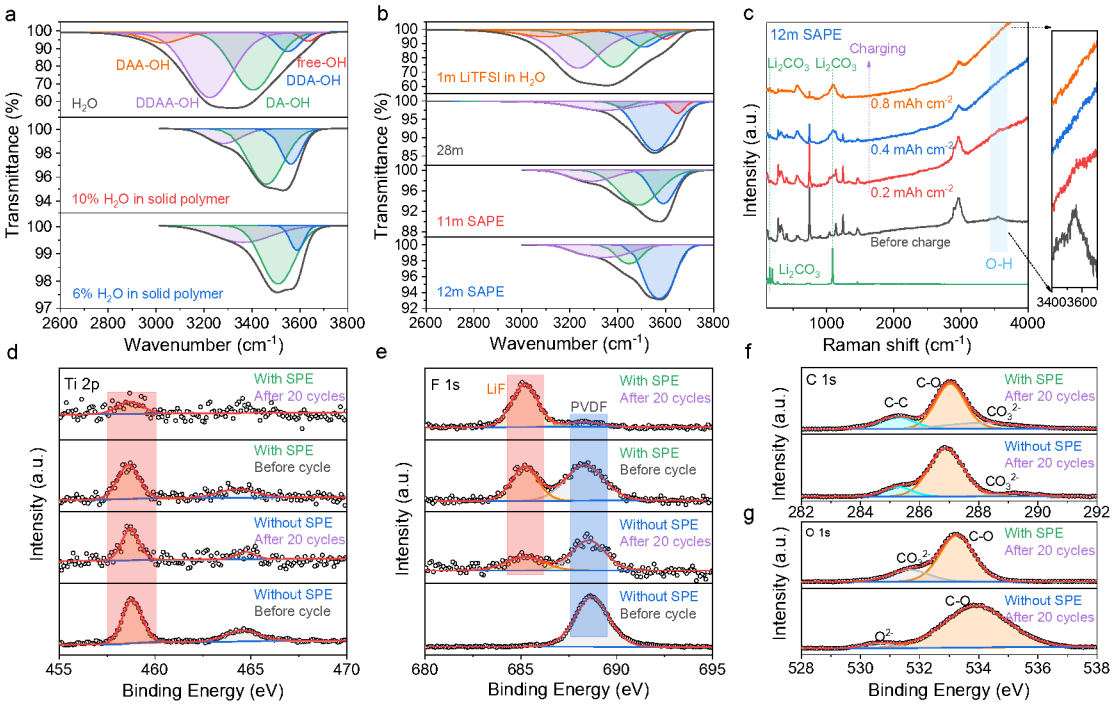

Figure 3 FTIR characterizations of electrolyte, Raman and XPS characterizations of SEI between anode and electrolytes. (a-b) The FTIR spectras observed in the range of 2,600-3,800 cm^{-1} correspond to the O-H stretching modes of water molecules. The O-H stretch bands were broken down into Gaussian peaks supposedly corresponding to hydrogen-bonded water molecules with different donor and acceptor hydrogen bonds. (c) *In-situ* Raman spectra of 12m SAPE/FTO anode interface at 1.7 V, showing spontaneous formation of water-less passivation layer and accumulation of Li_2CO_3 as a major composition of SEI layer. The interface was simulated by applying a constant voltage (1.7 V vs. Li/Li^+) on fluorine doped tin oxide (FTO) glass as transparent electrode. (d-g) XPS Ti 2p (d) F 1s (e), C 1s (f), and O 1s (g) spectra of the LTO anode before cycle and after 20 cycles with 12m SAPE or 12m SAPE@SPE as electrolyte, showing the detailed composition of SEI layer (LiF, Li_2CO_3). The solid polymer electrolyte layer and SAPE were carefully removed.

In addition to reduce the water activity by salt and polymer, the solid electrolyte interphase (SEI) also formed on anode in WiSE due to the reduction of salt as reported before.[29] Raman spectroscopy is used to monitor the water reduction and SEI formation on a transparent fluorine doped tin oxide (FTO) glass anode coupling with a $LiMn_2O_4$ (> 3 mAh cm^{-2}) counter electrode. The FTO anode in FTO/SAPE/LMO cell is discharged at a constant potential of 1.7 V (vs.

Li/Li$^+$) to mimic LTO anode in LMO//LTO cell, while Raman beam is focus on the interface at FTO/SAPE to in situ monitor water consumption and SEI formation. Fig. 3c shows that *in-situ* Raman spectra of 12m SAPE/FTO interface. The Raman laser is set to focus on the FTO/12m SAPE interface. The pristine sample (before charging) presents a featured band (~ 3560 cm^{-1}, similar as FTIR results) of water. After being charged to 0.8 mAh cm^{-2}, the water signal totally disappeared. Therefore, the side reaction (water decomposition) in initial cycle consumes the water in the interface layer of 12m SAPE, forming a water-less thin passivation interface on electrode and extending the window. Meanwhile, a peak of Li_2CO_3 is detected at the interface with charging proceed, which can be attributed to the formation of SEI on FTO. The formation of water-less thin Li_2CO_3 SEI during the first charge enhanced the Coulombic efficiency. Still, the formation of this water-free layer in the initial cycle would consume Li^+ ion from cathode in a full cell, which compromised the overall capacity. To enhance this strategy, a basic water-free PEO-LiTFSI-KOH SPE layer pre-coated on anode can further reinforce the Coulombic efficiency and the high local pH can also promote the LiTFSI reduction forming LiF SEI.[16]

XPS is used to further investigate the SEI composition formed on the surface of LTO anodes in the LMO//LTO full cells using 12m SAPE with and without PEO-LiTFSI-KOH SPE coating. The LTO with PEO-LiTFSI-KOH SPE layer coating is denoted as 'With SPE', no SPE pre-coating is denoted as 'Without SPE'. For the LTO without SPE layer, the Ti 2p XPS peak signal at 458.6 eV is very strong before cycling and the peak intensity become weaken after 20 charge/discharge cycles. The Ti 2p XPS peak at 458.6 eV corresponding to Ti in LTO electrode material, which indicates that the surface of LTO anode is covered by SEI after cycling (Fig. 3d). From the F 1s XPS peak (Fig. 3e), a peak at 685.2 eV corresponding to F^- in LiF is detected after cycling, while a peak at 688.5 eV results from the PVDF binder in the composite electrode. Meanwhile, a peak of C 1s at 288.9 eV corresponds to CO_3^{2-} is also formed on LTO surface (Fig. 3f), which is consistent with Raman analysis that Li_2CO_3 SEI is also formed on LTO surface. The formation of LiF-Li_2CO_3 SEI can effectively extends the electrochemical stability window of WiSE.[29]

When a water-free basic SPE layer (PEO-LiTFSI-KOH) was coated on LTO anode, the Ti 2p XPS peak signal is weaker than the LTO without SPE layer coating (Fig. 3d), which

means something came from the SPE layer remained on LTO anode. Interestingly, F 1s XPS peak at 685.2 eV corresponding to LiF is detected before cycling, which suggests that LiF immediately forms on LTO anode upon the coating of basic water-free SPE layer without any electrochemical process. It has been reported by Dubouis et al.[16] that hydroxides can chemically react with TFSI anions through a nucleophilic attack process and catalyze the formation of a fluorinated solid electrolyte interphase. Thus, the existence of KOH contributes to the decomposition of LiTFSI in the formation of LiF on the anode surface. After 20 cycles, the Ti 2p XPS peak signal is virtually vanished, illustrating the surface of LTO is completely covered by SEI. Simultaneously, the F 1s XPS peak signal at 688.5 eV stem from the PVDF binder in the composite electrode is also vanished. A very strong F 1s XPS peak signal at 685.2 eV corresponding to LiF is presented, indicating the formation of massive LiF on the surface of LTO. At the same time, the C 1s peak at 288.9 eV and O 1s peak at 531.6 eV corresponds to metal carbonates (Li_2CO_3), which is in consistent with the research before.[30, 31] The Li 1s XPS peak signal is presented in Fig. S6b (ESI†). A peak at 56.18 eV is close to the binding energy of LiF, another peak at 55.43 eV is close to the binding energy of Li_2CO_3. Thus, the Li 1s XPS signal further confirmed the existence of LiF and Li_2CO_3 in the SEI layer. Combining the XPS result of Ti 2p signal, a dense SEI layer composed of LiF and Li_2CO_3 is formed on the surface of LTO anode. As reported in previous research,[32, 33] dense and robust LiF SEI on the LTO surface can block the water effectively. Moreover, LiF-Li_2CO_3 composite has a much better Li-ion conductivity than LiF and Li_2CO_3.[29] Accordingly, with the corporation of these two compositions in SEI, the Coulombic efficiency of LTO anode enhanced significantly. Also, as presented in Fig. 3f, g, the SEI layer is composed of some organic compounds contain C-O and C-C groups, which originate from the reduction of polymer on anode surface.

Electrochemical performance of capacity matched full cell

The LMO//LTO full Li-ion cell with practical capacity ratio (LMO/LTO) of 1.14 and areal capacity of 0.5 mAh cm^{-2} is assembled to evaluate the electrochemical performance in different electrolytes. The slightly higher capacity of LMO than that of LTO is to compensate the irreversible Li consumption during the formation of SEI in initial cycles. Here, we utilize a low rate of 0.5 C to evaluate the authentic stability of aqueous electrolyte. The cycling

performances of LMO//LTO full cell with 28m WiSE, 11m SAPE, 12m SAPE and 12m SAPE@SPE electrolytes are presented in Fig. 4a, 4b and Fig. S7 (ESI†). The discharge capacity of LMO//LTO full cell decays rapidly to 37% of initial capacity after 5 cycles in 28m WiSE owing to the low Coulombic efficiency (< 70%). With the incorporation of polymer, the discharge capacity of LMO//LTO full cell in 11m SAPE decreased to 100 mAh g^{-1} (of LTO mass) after 20 cycles. The discharge capacity of LMO//LTO full cell in 12m SAPE retains at 125 mAh g^{-1} $_{(LTO)}$ after 100 cycles, with a high CE of 99.8%. For the LMO//LTO full cell with 12m SAPE@SPE electrolyte, a highest discharging capacity of 158 mAh g^{-1} $_{(LTO)}$ is achieved. The high CE of 90.5% in the first cycle is attributed to *in-situ* formation of SEI layer on LTO anode. To the best of our knowledge, this is the highest initial CE compared to the state-of-the-art aqueous electrolyte full cell systems reported so far. The dense SEI components formed in the first several cycles stabilize the LTO surface, and enable the CE increased to nearly 99.9% after only 20 cycles (Fig. 4b). After 200 cycles, the discharge capacity remains at ~142 mAh g^{-1} $_{(LTO)}$, with the CE reaching 99.95%, showing an excellent cycling stability. The corresponding voltage profiles of LMO//LTO full cell in 12m SAPE@SPE electrolyte are exhibited in Fig. 4c. The charge-discharge curves of LMO//LTO full cell in 12m SAPE@SPE electrolyte is the same as the behavior of LMO//LTO in non-aqueous electrolyte,[34] of which a voltage plateau at 2.5 V/2.6 V is observed during discharging/charging processes, respectively. The LMO//LTO full cell with 12m SAPE@SPE electrolyte achieves a high energy density of 151 Wh kg^{-1} (60.5 Ah kg^{-1}, 2.5 V average discharge potential) based on the total mass of LMO and LTO, and maintained 131 Wh kg^{-1} (54.5 Ah kg^{-1}, 2.4 V average discharge potential) even after 200 cycles (Fig. S8, ESI†). At a high C rate (1 C), the LMO//LTO full cell shows exceptional cycling stability with capacity decay rates per cycle of 0.034% for 600 cycles, with an average CE of 99.97%, which is comparable to non-aqueous Li-ion cells.[35] Here, we presented the optimization process of monomers' weight ratio and Pyr_{13} TFSI's molar ratio within the SAPE electrolyte in Fig. S9, S10 and Table S2, S3 (ESI†).

The rate capability of LMO//LTO full cell with 12m SAPE or 12m SAPE@SPE electrolyte is evaluated in Fig. 4e. At a low rate of 0.2 C, the discharge capacity of LMO//LTO full cell with 12m SAPE reached to 160 mAh $g^{-1}$$_{(LTO)}$. However, the low CE of 95% cause a quick capacity decay, which is different from the capacity behavior of LMO//LTO at a high

rate of 0.5 C (Fig. 4a) where the capacity is slightly low (150 mAh g^{-1}), but cycle is more stable. Therefore, the SEI is more easily formed in relatively high rate. With the current density increases, the LMO//LTO full cell with 12m SAPE maintains the discharge capacity of 130 mAh g^{-1} $_{(LTO)}$ at 0.5 C (0.075 A g^{-1}) and 127 mAh g^{-1} $_{(LTO)}$ at 2 C (0.3 A g^{-1}). In sharp contrast, the LMO//LTO full cell with 12m SAPE@SPE electrolyte delivers a much higher CE at 0.2 C, a discharge capacity of 147 mAh g^{-1} $_{(LTO)}$ after 10 cycle presents at 0.2 C. With the current density increases, it maintained the discharge capacity of 147 mAh g^{-1} $_{(LTO)}$ at 0.5 C (0.075 A g^{-1}) and 141 mAh g^{-1} $_{(LTO)}$ at 2 C (0.3 A g^{-1}), which are much higher than that of 12m SAPE. After the rate capability recovered to 0.2 C (0.03 A g^{-1}), the discharge capacity returned to 144 mAh g^{-1} $_{(LTO)}$ revealing an excellent rate performance, and much better than typical solid polymer electrolyte in full cells.[21]

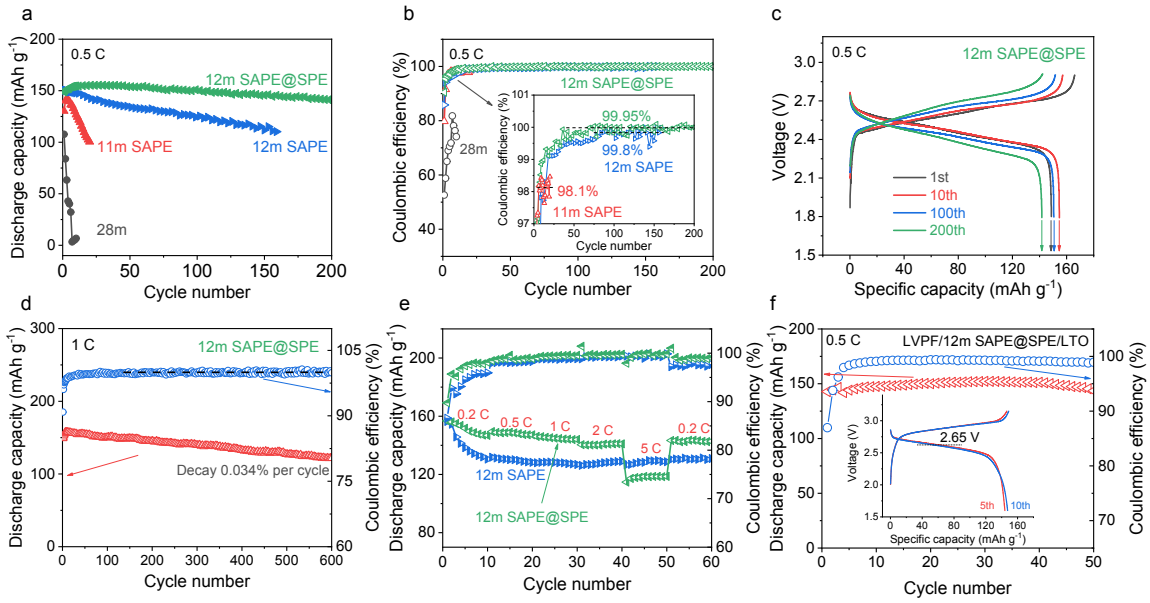

Figure 4 Electrochemical performance of capacity matched LMO//LTO full cell and LVPF//LTO full cell. Cycling stability (a) and Coulombic efficiency (b) of LMO//LTO full cell in 28m WiSE, 11m SAPE, 12m SAPE and 12m SAPE@SPE electrolyte at 0.5 C. (c) The voltage profiles of 1st, 10th, 100th and 200th cycling of LMO//LTO full cell in 12m SAPE@SPE electrolyte at 0.5 C (0.075 A g^{-1} for LTO, based on mass of LTO). (d) Cycling stability and Coulombic efficiency of LMO//LTO full cell in 12m SAPE@SPE electrolyte at 1 C. (e) The rate capability of LMO//LTO full cell in 12m SAPE and 12m SAPE@SPE electrolyte at room temperature. (f) Cycling stability, Coulombic efficiency and voltage profiles (inset) of LVPF//LTO full cell in 12m SAPE@SPE electrolyte at 0.5 C.

To fully use the high anode potential limit (4.86V) of solid-state aqueous polymer electrolyte system, high potential $LiVPO_4F$ (LVPF) was used as cathode to couple with LTO.

The electrochemical performance of LVPF//LTO full Li-ion cell with a areal capacity of 0.5 mAh cm^{-2} and P/N capacity ratio of 1.4 is evaluated at 0.5 C in 12m SAPE@SPE electrolyte. The cycling performances and voltage profiles are presented in Fig. 4f. The capacity ratio of LVPF/LTO is 1.4. After 3 formation cycles, the discharge capacity reaches a steady value of 152 mAh g^{-1}. The Coulombic efficiency is close to 99.3% for the LVPF//LTO full cell. The discharge platform voltage is close to 2.65 V. Thus, the energy density further enhanced with the cooperation of LVPF and LTO.

The electrolyte flammability and LMO//LTO cell flexibility were also evaluated. Previous reports have proved that 28m WiSE is non-flammable, and the ion liquids Pyr_{13} TFSI exhibit both non-volatility and non-flammability.[18] As revealed in Fig. S11 and Video S2 (ESI†), after remove the fire from the 12m SAPE sample, the electrolyte won't keep combustion, presenting excellent safety performance owing to the intrinsically safe nature of water. As shown in Fig. S12a (ESI†), LMO//LTO cell holds almost the same capacity after bend the cell to 45°, 90°, 135° and 180°, and negligible capacity is lost even after bended the cell for over 200 times (Fig. S12b, ESI†), confirming the excellent flexibility. Video S3 (ESI†) shows the robustness of LMO//LTO cells under ambient air and water environment. As revealed, the flexible pouch cell with capacity of 100 mAh (Fig. S13, ESI†) successfully powered the mini-fan, of which requires a power around 160 mW. Moreover, after cut the flexible pouch cell in ambient air and water, no catastrophic cell failure is detected in this process with the fan keep working. Benefit from the strong bonding of the polymer network, which keeps the water and salt in the framework of polymer, the aqueous SAPE can withstand cutting and continue to operate in an open cell condition even in water environment without failure. The outstanding safety performance of this newly developed aqueous electrolyte opens a door for the application of lithium-ion battery.

A 3 cm × 4 cm size LMO//LTO pouch cell with capacity ratio (LMO/LTO) of 1.14 and areal capacity of 0.5 mAh cm^{-2} is assembled to evaluate the electrochemical performance in the 12m SAPE@SPE electrolyte. The cycling performance of large scale pouch cell is presented in Fig. 5a. A low C rate of 0.2 C is applied on the pouch cell to fully use the active material for 5 cycles, after this formation process, we use 0.5 C for cycling process. A high capacity of 5.9 mAh can be reached for this pouch cell. The discharge capacity of LMO//LTO pouch cell in

12m SAPE@SPE remained around 94 % after 50 cycles. The corresponding voltage profiles of LMO//LTO pouch cell in 12m SAPE@SPE are presented in the inset of Fig. 5a. The charge-discharge curves of the pouch cell are similar with the coin cells. To increase the energy density, we increased the loading of active material of LMO//LTO cells to 1.5 mAh cm^{-1}. The cross-section SEM image of high loading LTO electrode is presented in Fig. S14 (ESI†). The thickness of the LTO electrode is around 86 μm. The electrode area is 1.98 cm^2. The electrochemical performance is shown in Fig. 5b. The voltage profiles of the high loading LMO//LTO full cell in 12m SAPE@SPE electrolyte at 0.2 C are the same as the low loading cells. The capacity of LMO//LTO cells in the first several cycle is close to the theoretical capacity of the cell (3 mAh cm^{-1}), which demonstrate a good wetting ability of the SAPE electrolyte into the electrode. Moreover, the UV-curved solid-state aqueous polymer electrolytes have a high mechanical strength and can function as a binder to fabricate a thick electrode in solid state batteries. Remarkably, we demonstrate a thick electrode using UV-curved SAPE as binder. By mixing LTO with 12m SAPE with the ratio of 1:1, and curing under the UV light for 90 secs, we successfully fabricated the LTO-SAPE electrode with a high loading of 40 mg cm^{-2} and 200 μm thick. The cross-section SEM image of the fabricated LTO-SAPE electrode is presented in Fig. S15 (ESI†). The LTO-SAPE electrode paved the way for the development of high energy solid state battery.

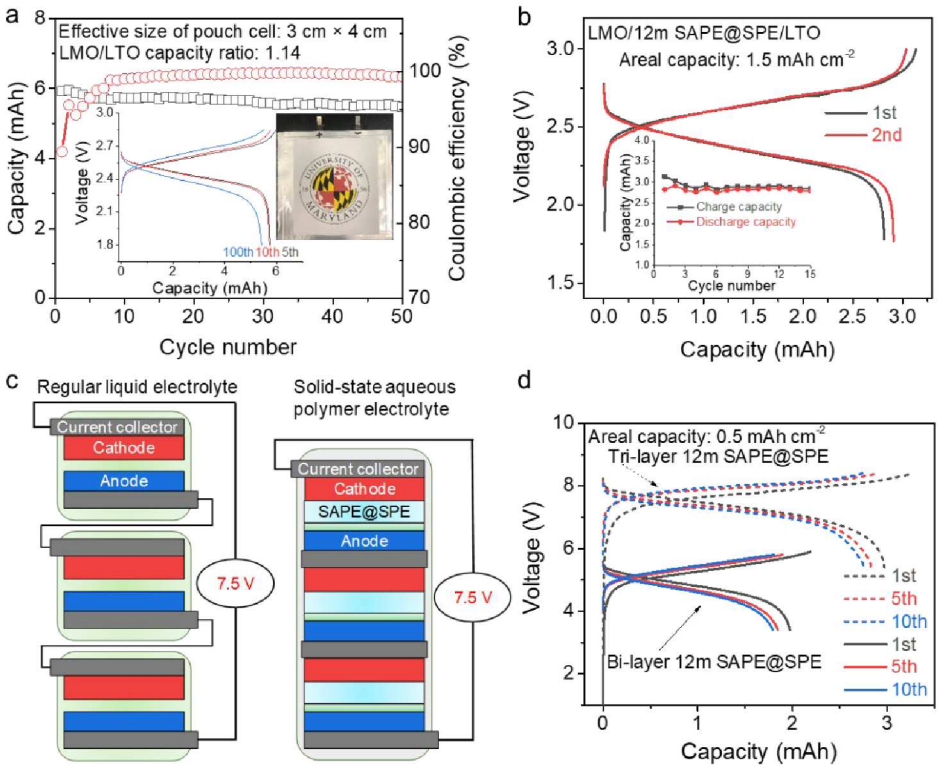

Figure 5 Electrochemical performance of large scale LMO//LTO full cell, high active material loading full cell and bipolar cell. (a) Cycling stability, Coulombic efficiency and voltage profiles (inset) of LMO//LTO pouch cell in 12m SAPE@SPE electrolyte at 0.5 C. (b) Cycling stability (inset) and voltage profiles of LMO//LTO full cell with loading amount of 1.5 mAh cm^{-1} active material in 12m SAPE@SPE electrolyte at 0.2 C. (c) Schematic structure of tri-layered bipolar stacked LMO//LTO cell. (d) The voltage profiles of bi-layered and tri-layered bipolar LMO//LTO coin cell with 12m SAPE@SPE electrolyte at 0.2 C.

The solid-state aqueous polymer electrolytes provides a technical solution to address the safety problems of lithium-ion batteries and enables a bipolar design of high-voltage and high-energy battery modules. Here, we designed a multilayered bipolar cell stacked with 12m SAPE@SPE electrolytes, which avoids the use of some passive components and parts required for packaging and external electrical connection. Hence, the bipolar design facilitates an increase in the volumetric energy density of the battery, while enables easy build-up of high output voltage. Fig. 5c presents the structure of a multilayered bipolar stacked solid-state aqueous polymer electrolyte lithium-ion battery. The bipolar stacked solid-state batteries were fabricated by layering two or three solid-state batteries and trapping them in the CR2032 module coin cell. Fig. 5d shows the voltage profiles of the bi-layered and tri-layered solid-state LMO//LTO full cell at 0.2 C, respectively. The plateau potential of the bi-layered and tri-

layered battery is 4.9 V and 7.4 V, respectively, which is close to two and three times than that of the single-layered battery (2.5 V), confirming that the cell package did not have internal short-circuits and operated successfully.

Conclusions

A solid-state aqueous polymer electrolyte was developed by curing WiSE into the network of methacrylic polymer. The obtained SAPE electrolytes exhibit higher ionic conductivity compared with traditional solid polymer electrolyte. Comparing the research of ionic liquids reported before, the ion transport property enhanced with the cooperation of WiSE. The activity of water molecules were further stabilized in the polymer network by the cross-linked solid-state polymer and highly-concentrated salt. LiF-Li_2CO_3 SEI was formed during initial charge/discharge cycles, which suppressed water reduction in the late cycles. To further reduce the water reduction in the first few cycles, a water-free thin PEO-LiTFSI-KOH SPE interface was inserted between anode and electrolyte to further enhance the Coulombic efficiency. The 12m SAPE@SPE electrolyte achieves a wide electrochemical stability window of 3.86 V. The $LiMn_2O_4$//$Li_4Ti_5O_{12}$ full cell with practical capacity ratio of 1.14 and 12m SAPE@SPE electrolyte exhibited unprecedented high initial Coulombic efficiency of 90.50% and average Coulombic efficiency of 99.95% at low 0.5 C. The full cell's energy can be enhanced by increasing active material's area capacity to 1.5 mAh cm^{-1}. A large scale $LiMn_2O_4$/12m SAPE@SPE/ $Li_4Ti_5O_{12}$ pouch cell has similar cycle capability with the corresponding coin cell. The pouch cell maintains high performance after bending with different angles and times, and cutting in air and in water. An ultra-thick LTO electrode with 12m SAPE as binder is also demonstrated as solid state battery electrode. And a high-voltage (7.4 V) solid-state bipolar cell is assembled with 12m SAPE@SPE electrolyte. The flexible separator-free SAPE LMO//LTO cells with super robustness can be widely used for low-cost and high-safety flexible electronic devices.

Author contributions

J.Z., C.Y. and C.W. conceived the idea of the study. J.Z., C.C. and P. W. prepared the materials and conducted the electrochemical experiments. Q.L., L.C., F.H., T.J., S.L., N.E., A.C. and

L.M. analyzed the data. H.C. and S.R. performed the Rhegological test. J.U. and D.A. performed the In-situ cell pressure and Mass spectra test. J.Z., C.C, P.W., C.Y. and C.W. wrote the paper, and all the authors contributed to the interpretation of the results. J. Z., C. C. and P. W. contribute equally to this work.

Conflicts of interest

There are no conflicts to declare.

Acknowledgements

The authors gratefully acknowledge funding support from the US Department of Energy (DOE) through ARPA-E grant (DEAR0000389), U.S. Army Research Laboratory (W911NF1920341) and the Center of Research on Extreme Batteries. J.Z. acknowledges fellowship from the China Scholarship Council (grant no. 201706320341). We also acknowledge the support of the Maryland Nano Center and its NispLab. The NispLab is supported in part by the NSF as a MRSEC Shared Experimental Facility.

References

1. L. Suo, O. Borodin, T. Gao, M. Olguin, J. Ho, X. Fan, C. Luo, C. Wang and K. Xu, *Science*, 2015, **350**, 938-943.
2. Y. Yamada, K. Usui, K. Sodeyama, S. Ko, Y. Tateyama and A. Yamada, *Nature Energy*, 2016, **1**, 16129.
3. C. Yang, J. Chen, T. Qing, X. Fan, W. Sun, A. von Cresce, M. S. Ding, O. Borodin, J. Vatamanu, M. A. Schroeder, N. Eidson, C. Wang and K. Xu, *Joule*, 2017, **1**, 122-132.
4. C. Yang, J. Chen, X. Ji, T. P. Pollard, X. Lü, C.-J. Sun, S. Hou, Q. Liu, C. Liu, T. Qing, Y. Wang, O. Borodin, Y. Ren, K. Xu and C. Wang, *Nature*, 2019, **569**, 245-250.
5. G. Xu, X. Shangguan, S. Dong, X. Zhou and G. Cui, *Angewandte Chemie International Edition*, 2020, **59**, 3400-3415.
6. L. Suo, O. Borodin, W. Sun, X. Fan, C. Yang, F. Wang, T. Gao, Z. Ma, M. Schroeder, A. von Cresce, S. M. Russell, M. Armand, A. Angell, K. Xu and C. Wang, *Angewandte Chemie International Edition*, 2016, DOI: 10.1002/anie.201602397, n/a-n/a.
7. C. Yang, X. Ji, X. Fan, T. Gao, L. Suo, F. Wang, W. Sun, J. Chen, L. Chen, F. Han, L. Miao, K. Xu, K. Gerasopoulos and C. Wang, *Advanced materials*, 2017, **29**, 1701972.
8. Y. Tamai, H. Tanaka and K. Nakanishi, *Macromolecules*, 1996, **29**, 6750-6760.
9. D. Capitani, V. Crescenzi, A. De Angelis and A. Segre, *Macromolecules*, 2001, **34**, 4136-4144.
10. L. T. Ng, J. T. Guthrie, Y. J. Yuan and H. Zhao, *Journal of Applied Polymer Science*, 2001, **79**, 466-472.
11. E. H. Kil, K. H. Choi, H. J. Ha, S. Xu, J. A. Rogers, M. R. Kim, Y. G. Lee, K. M. Kim, K. Y. Cho and S. Y. Lee, *Advanced materials*, 2013, **25**, 1395-1400.
12. Y. H. Chang, C. W. Ku, Y. H. Zhang, H. C. Wang and J. Y. Chen, *Advanced Functional Materials*, 2020, **30**,

2000764.
13. C. Decker, *Polymer International*, 1998, **45**, 133-141.
14. J. Nair, C. Gerbaldi, G. Meligrana, R. Bongiovanni, S. Bodoardo, N. Penazzi, P. Reale and V. Gentili, *Journal of Power Sources*, 2008, **178**, 751-757.
15. J. R. Nair, C. Gerbaldi, M. Destro, R. Bongiovanni and N. Penazzi, *Reactive and Functional Polymers*, 2011, **71**, 409-416.
16. N. Dubouis, P. Lemaire, B. Mirvaux, E. Salager, M. Deschamps and A. Grimaud, *Energy & Environmental Science*, 2018, **11**, 3491-3499.
17. X. Shen, Y. Li, T. Qian, J. Liu, J. Zhou, C. Yan and J. B. Goodenough, *Nature communications*, 2019, **10**, 1-9.
18. J. M. Klein, E. Panichi and B. Gurkan, *Physical Chemistry Chemical Physics*, 2019, **21**, 3712-3720.
19. L. Chen, J. Zhang, Q. Li, J. Vatamanu, X. Ji, T. P. Pollard, C. Cui, S. Hou, J. Chen and C. Yang, *ACS Energy Letters*, 2020, **5**, 968-974.
20. K. Xu, *Chemical Reviews*, 2004, **104**, 4303-4418.
21. D. Lin, W. Liu, Y. Liu, H. R. Lee, P.-C. Hsu, K. Liu and Y. Cui, *Nano letters*, 2015, **16**, 459-465.
22. G. Chen, F. Zhang, Z. Zhou, J. Li and Y. Tang, *Advanced Energy Materials*, 2018, **8**, 1801219.
23. S. Gharazi, B. C. Zarket, K. C. DeMella and S. R. Raghavan, *ACS Appl Mater Interfaces*, 2018, **10**, 34664-34673.
24. I. Belharouak, G. M. Koenig, T. Tan, H. Yumoto, N. Ota and K. Amine, *Journal of the electrochemical society*, 2012, **159**, A1165-A1170.
25. C. Yang, L. Suo, O. Borodin, F. Wang, W. Sun, T. Gao, X. Fan, S. Hou, Z. Ma, K. Amine, K. Xu and C. Wang, *Proc Natl Acad Sci U S A*, 2017, **114**, 6197-6202.
26. Q. Sun, *Vibrational Spectroscopy*, 2009, **51**, 213-217.
27. C. Choe, J. Lademann and M. E. Darvin, *Analyst*, 2016, **141**, 6329-6337.
28. O. Borodin, L. Suo, M. Gobet, X. Ren, F. Wang, A. Faraone, J. Peng, M. Olguin, M. Schroeder, M. S. Ding, E. Gobrogge, A. von Wald Cresce, S. Munoz, J. A. Dura, S. Greenbaum, C. Wang and K. Xu, *ACS Nano*, 2017, **11**, 10462-10471.
29. L. Suo, D. Oh, Y. Lin, Z. Zhuo, O. Borodin, T. Gao, F. Wang, A. Kushima, Z. Wang and H.-C. Kim, *Journal of the American Chemical Society*, 2017, **139**, 18670-18680.
30. C. Yang, X. Ji, X. Fan, T. Gao, L. Suo, F. Wang, W. Sun, J. Chen, L. Chen and F. Han, *Advanced materials*, 2017, **29**, 1701972.
31. A. Shchukarev and D. Korolkov, *Open Chemistry*, 2004, **2**, 347-362.
32. L. Zhang, K. Zhang, Z. Shi and S. Zhang, *Langmuir*, 2017, **33**, 11164-11169.
33. J. Ko and Y. S. Yoon, *Ceramics International*, 2018.
34. Z. Wu, Y. Wang, X. Liu, C. Lv, Y. Li, D. Wei and Z. Liu, *Advanced materials*, 2019, **31**, 1800716.
35. B. Gangaja, K. S. Reddy, S. Nair and D. Santhanagopalan, *ChemistrySelect*, 2017, **2**, 9772-9776.